2008 IEEE International Conference on
Robotics and Automation
Pasadena, CA, USA, May 19-23, 2008

Micro Rotary-Linear Ultrasonic Motor for Endovascular Diagnosis and Surgery

Tomoaki Mashimo, *Student Member, IEEE*, and Shigeki Toyama, *Member, IEEE*

Abstract— **We present a micro ultrasonic motor having rotary and linear motions (rotary-linear motor) suitable for endovascular diagnosis and surgery. The rotary-linear motor is miniaturized to the size needed to function in a blood vessel. The stator prototype is a cube of side 3.5mm, and the main body is fabricated as a single metallic cube with a through-hole. Four piezoelectric elements are bonded to the sides of the stator. When AC voltage at each resonant frequency is applied to the piezoelectric elements, the circumference of the stator generates elliptical motions at each natural frequency. We can obtain the output from a shaft inserted through the hole. We developed the first prototype of the stator using the finite element method (FEM), and experimentally determined the output of the rotary-linear motor. In the rotary sense, approximately 260 rpm and 0.1 mNm were attained at a resonant frequency of 270 kHz, and in the linear sense about 50 mm/s and 0.01 mN was attained at 306 kHz by driving the system at applied voltages of 42 V_{rms}.**

I. INTRODUCTION

Endovascular surgery is a method of minimally invasive surgery that is capable of accessing many regions of the body via blood vessels. Most endovascular techniques involve the percutaneous insertion of a catheter through the skin into a large blood vessel. Typically, the chosen blood vessel is the femoral artery or vein. The catheter is injected with a radio-opaque contrast medium visible on live x-ray. As the contrast medium courses through the blood vessels, diagnosis images can be observed by experienced viewers. This procedure assists in the diagnosis of diseases such as thrombosis.

Much research is focused on the use of mechanical and electronic devices for endovascular surgery. The catheter has so far been manipulated by a guide wire reaching sufficiently far to choose a branch of vessels. An active catheter is an attractive research goal, which can bend so as to select a desired branch. Guo et al. reported an active catheter using Ionic Conducting Polymer Film (ICPF) Actuator [1]. The ICPF bend the catheter by applying a low voltage, of approximately 1V. Haga et al. are developing an active catheter using shape memory alloy (SMA) [2]. SMA has superior energy density. Ikuta has developed an active catheter using hydraulic pressure [3]. Its advantage is safety, because no voltages are applied.

Recently several rotational devices, called atherectomy [4], have been used for the endovascular surgery. The rotablator has a diamond burr at the tip of catheter. After it was guided to the blockage, the diamond burr rotates at high speeds. The burr grinds the hardened plaque into small particles. Directional atherectomy was designed to remove non-calcified plaque. After insertion of the catheter, a balloon inflates, pushing the blade toward the plaque. The blade cuts away the plaque and stores it in a chamber. The balloon deflates and the plaque is removed when the catheter is withdrawn. Intravascular ultrasound (IVUS) was used for the diagnosis. IVUS is a medical imaging method with an ultrasound probe attached to the tip end of the catheter. The most valuable use of IVUS is to see the plaque, which is not visible by angiography. Wada et al. report a rotational actuator using ultrasonic vibration [5]. A cylindrical rotor with a mirror rotates, for diagnosis of the vessel wall. The advantage of the system is that the motor can rotate in a vessel without applied voltages, because the ultrasonic vibrations are transferred from the outside the human body. These devices are rotated by wire using a driving source including a rotational motor outside the human body. In the catheters, the rotary motion is a transfer from the driving source, and the linear motion is manipulation by a human hand. In a complex and narrow blood vessel, the use of the devises should be difficult because of the buckling and the inflexibility of the catheter.

Accordingly, we present a novel small ultrasonic motor having rotary and linear motions. The ward "ultrasonic" means the frequency range of the applied voltages to the piezoelectric elements. An image of its application in endovascular surgery is shown in Fig. 1. Although there are many researches on miniature actuators, they only have either rotary or linear motion [6]-[8]. The catheter using the several small motors generates the rotary and linear motions in the case of that the catheter is bending along blood vessel. The stator is fabricated as a rectangular metallic solid with a

This work was supported in part by a grant-in-aid from JSPS Research Fellowships for Young Scientists, JSPS under a Grant-in-Aid for Scientific Research (B) 19360071, Electro- mechanic Technology Advancing Foundation, Mazak Foundation.

Tomoaki Mashimo is with the Department of Mechanical System Engineering, Tokyo University of Agriculture and Technology, 2-24-16 Nakacho, Koganei-city, Tokyo 184-8588, Japan. (Corresponding author: Phone: +81-42-388-7098; Fax: +81-42-388-7098; E-mail: t-masimo@ cc.tuat.ac.jp).

Shigeki Toyama is with the Institute of Symbiotic Science and Technology, Tokyo University of Agriculture and Technology, Tokyo, Japan. (E-mail: toyama@ cc.tuat.ac.jp).

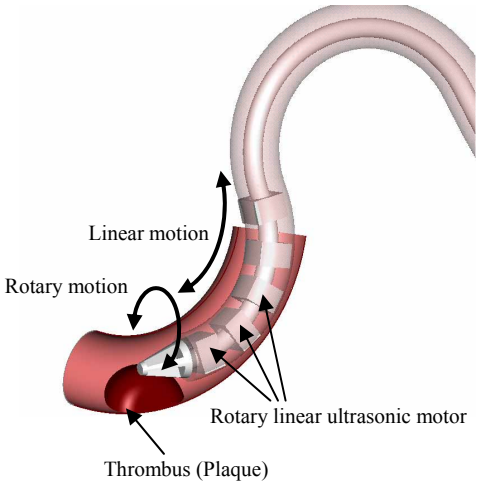

Fig.1 Aterectomy catheter using the rotary linear ultrasonic motor

through-hole. The shape of the stator makes the machining easy and inexpensive. This simple structure is suitable to be miniaturized for endovascular operation. Additionally, the micro rotary-linear motor has magnetic resonance imaging (MRI) compatibility. MRI, which involves a strong magnetic field, employs ultrasonic motors for moving its seat, or MRI compatible surgical robot researches [9]. MRI can eliminate exposure to radiation from computer tomography (CT) or side effect from the contrast medium. Although diagnostic X-rays provide great benefits, their use involves some small risk of inducing cancer [10]. In this paper, we describe the principle of the rotary-linear motor and the construction of a rotary-linear motor with a 3.5 mm cubic stator. Characteristics of the rotary-linear motor are measured.

II. Driving Principle of Rotary and Linear Motion

A. Driving principle

We explain the three vibration modes in the rotary-linear motor. The stator of rotary-linear motor excites distinct vibration modes in the case of rotary and linear motions. The hole of the stator generates each elliptical motion. In this paper, the "axis" is defined as the axis of the hole and is the z-axis, and the "radius" is defined as the radius of the hole of the stator. The mode of the rotary motion comprises three waves along the circumference of the through-hole (R_3 mode) as shown in Fig.2(a). The modes of linear motion are a first extension mode (T_1 mode), as shown in Fig.2(b), and a second extension mode (T_2 mode) in Fig.2(c). The node of the T_2 mode is median surface of the stator in perpendicular direction to the axis. The antinodes are eight corners. The two modes are excited at a single resonant frequency. Generation of the elliptical motion by the combination of the modes at a single resonant frequency has been reported by an ultrasonic linear motor [11], [12] and multi-degree of freedom ultrasonic motor [13], [14]. These involved a combination of

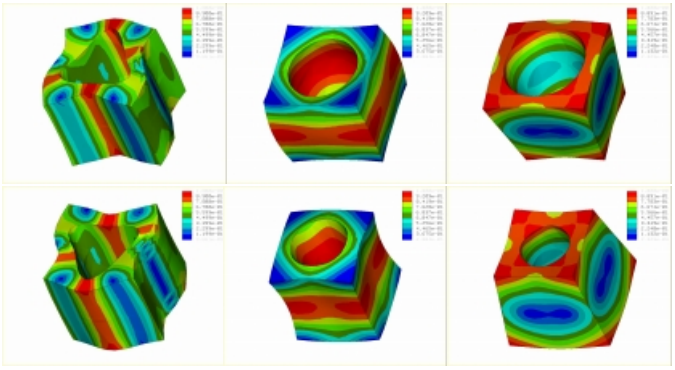

(a) R_3 mode (276 kHz) (b) T_1 mode (321 kHz) (c) T_2 mode (322 kHz)

Fig.2 Vibrational mode shapes of the rotary and linear motor

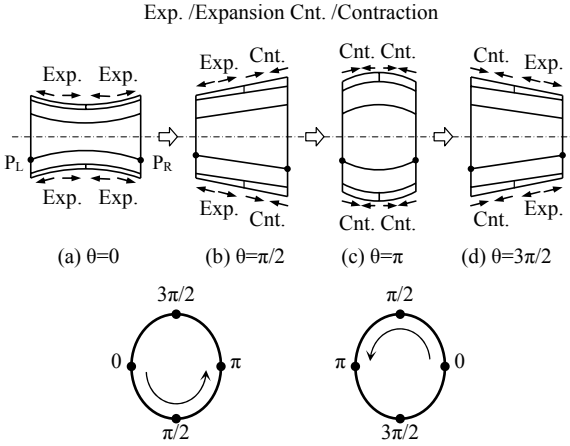

Fig.3 Trajectory of the elliptical motions

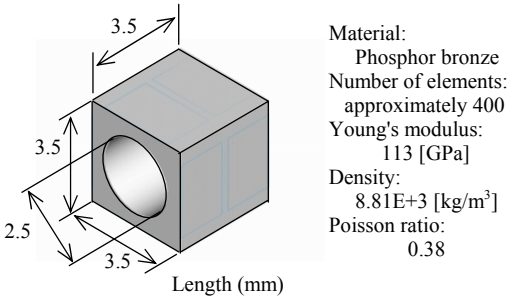

Fig.4 Model and parameters for FEM analysis

the first extension mode and the second bending mode of a free beam or plate.

In the stator of the rotary-linear motor, the elliptical motion is generated by the T_1 and T_2 modes. The sequence of the displacement is shown in Fig.3(a) to (d). The T_1 mode is a repeat of Fig.3 (a) and (c), and the T_2 mode is a repeat of Fig.3(b) and (d). The T_1 mode has symmetry and the T_2 mode has anti-symmetry with respect to the median surface. When the phase difference between T_1 mode and T_2 mode is $\pi/2$, the

elliptical motion is generated. The points P_L and P_R are located at either edges of inner surface in Fig.3(a). When the movement of the points is plotted, elliptical motion is drawn in the same direction as in Fig.3(e) and (f). The elliptical motion therefore moves the output shaft in the direction of the axis.

Characteristic analysis using finite element methods (FEM) clarifies the mode shapes and natural frequencies of the stator. The stator must be designed to have the natural frequencies such that the T_1 and T_2 modes accord. When the stator size is changed, the shift of the natural frequency is analyzed by FEM. The FEM model of the stator is shown in Fig.4; the material characteristics are those of phosphor bronze. The height H, width W, and depth (length in direction to the axis) L are all 3.5 mm. The diameter of the though hole is 2.5 mm. The number of elements in the FEM model is approximately 400. The natural frequency of R_3 mode was 276 kHz. The natural frequencies of T_1 mode and T_2 mode are respectively 321 kHz and 322 kHz, essentially identical as expected for the cubic shape.

B. Kinematics of the rotary-linear motor

The movement of the output shaft of the rotary-linear motor is expressed by cylindrical coordinates as shown in Fig.5(a), with the position vectors written as $\mathbf{P}=[\rho, \theta, z]$. The position of movement of the output shaft is expressed by two basis vector $\mathbf{u}_\theta$ and $\mathbf{u}_z$. Consider the case of that the preload and friction coefficient between the output shaft and the stator is given by N and μ, respectively. The generated elliptical motions transfer the energy by the friction to the output shaft as shown in Figs.5 (b) and (c). When the independent rotary or linear motion are driven, the torque $\mathbf{M}$ and thrust force $\mathbf{F}$ are expressed by

$$\mathbf{M} = I\ddot{\theta}\mathbf{u}_\theta \quad (1)$$

$$\mathbf{F} = m\ddot{z}\mathbf{u}_z \quad (2)$$

Where I is the moment of inertia in rotary direction, and m is the mass of the output shaft. In the micro ultrasonic motor, the torque has been calculated by the equation (1) because the torque is too small to measure directly by instrument [15]. The torque and thrust force will be calculated from experimental angular and linear accelerations by eqs. (1) and (2).

III. Experimental Setup

A. Prototype of the rotary-linear motor

A prototype rotary-linear motor was constructed as shown in Fig.6. The piezoelectric element (Material C-82: Fuji Ceramics Co., Japan) is shown in Fig.6 (a). It has two silver electrodes, the direction of which is polarized "positive" in one side. Another side is a silver electrode polarized "negative," this side is bonded to the side of the stator. The surface of the piezoelectric elements in contact with the stator

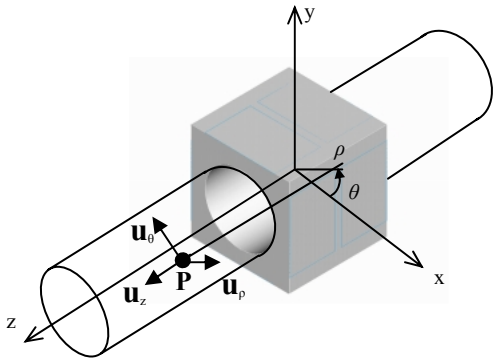

(a) Cylindrical coordinates in rotary-linear motor

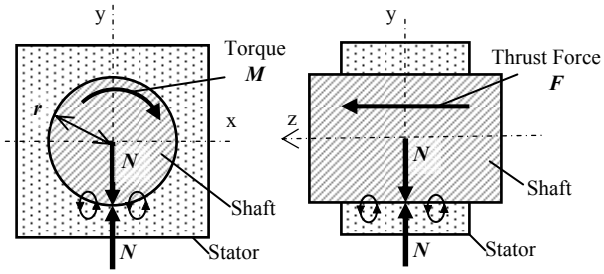

(b) Rotation (c) Translation

Fig.5 Mechanism of the rotary-linear motor

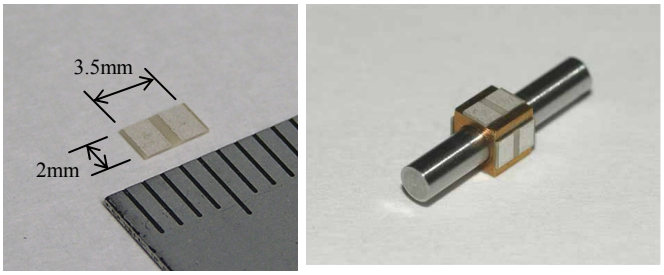

(a) Piezoelectric element (b) Prototyped rotary-linear motor

Fig.6 Prototype of rotary-linear motor

conducts electrically to the body of the stator, and also to ground. One of the prototype rotary-linear motor is shown in Fig.6(b). Four piezoelectric elements are bonded to the sides of the stator. Table 1 shows the experimental conditions for this prototyped rotary-linear motor. The measured clearance between the stator and the output shaft is approximately 10 μm. The inserted shaft can be moved by light force of hand. In the experiment, the size of the stator is a 3.5 mm cube with a hole of inner diameter 2.5 mm as in simulation in Fig.4.

The four sides of the stator are named "A" to "D" in direction to z-axis clockwise, and the positive direction of z-axis is called "p" and the negative direction is "n." Four piezoelectric elements are placed at the four sides of the stator. The amplitude of the AC voltages applied to all silver electrodes on these piezoelectric elements are given as "E_{Ap}", "E_{An}" to "E_{Dp}", "E_{Dn}" as shown in Fig.7. To generate the

Table 1 Experimental setup

Material of the output shaft	Stainless steel
Length of the output shaft	50 mm
Weight of the output shaft	1.84 g
Diameter of the output shaft	2.497mm
Average roughness of the shaft's surface	3.2 μm
Material of the stator	Phosphor bronze
Diameter of the hole	2.507mm
Average roughness of the hole's surface	3.2 μm

rotation, four voltages in phase step of π/2 are applied around the z-axis as given by

$$E_{Ap} = E_{An} = A\sin(2\pi f_r t) \quad (3)$$

$$E_{Bp} = E_{Bn} = A\sin(2\pi f_r t + \pi/2) \quad (4)$$

$$E_{Cp} = E_{Cn} = A\sin(2\pi f_r t + \pi) \quad (5)$$

$$E_{Dp} = E_{Dn} = A\sin(2\pi f_r t + 3\pi/2) \quad (6)$$

where A is the amplitude of the applied voltages, f_r is a natural frequency excites R_3 mode. Eqs. (3) to (6) represent a traveling wave. For generating translation, the applied voltages E_{Ap}, E_{An} to E_{Dp}, E_{Dn} are

$$E_{Ap} = E_{Bp} = E_{Cp} = E_{Dp} = A\sin(2\pi f_t t) \quad (7)$$

$$E_{An} = E_{Bn} = E_{Cn} = E_{Dn} = A\sin(2\pi f_t t + \pi/2) \quad (8)$$

where f_t is a natural frequency excites T_1 and T_2 modes. The amplitude of the voltages A is 42 V_{rms} in this experiment.

B. Measuring device

A schematic of setup for measuring the characteristics in rotary and linear motions are shown in Fig.8. The stator is lightly fixed on a holding component and the corner of the stator contacts the holding component, which connects to ground. The weight of the output shaft itself comprises the preload between the stator and the output shaft. The device measures rotation using a contactless rotary encoder (Mercury 1500, MicroE systems corp., U.S.A.) and measures linear motion by a contactless laser position sensor (Smart sensor ZX-LD40, Omron, Japan). Two weights are attached to the each edge of the output shaft to provide the preload between the shaft and the stator. The rotary scale of diameter 12 mm are attached an edge for measuring rotational speed. The preload is the sum of the two weights, output shaft, and the rotary scale. In the experiment this total weight is approximately 0.01 kg. When the output shaft with the rotary scale is rotated, the contactless rotary encoder can measure the rotational speed. For measuring the linear motion, the rotary encoder is removed from the device. The contactless linear sensor emits laser light to the shaft in the z-axis direction. The edge of the shaft reflects the light. By the triangulation principle, the linear sensor output the linear position of the shaft without any contact. If the change of rotary and linear positions for a few milliseconds is known,

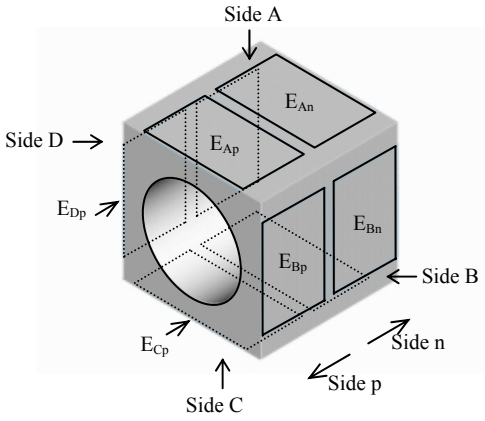

Fig.7 Electrode the voltages apply

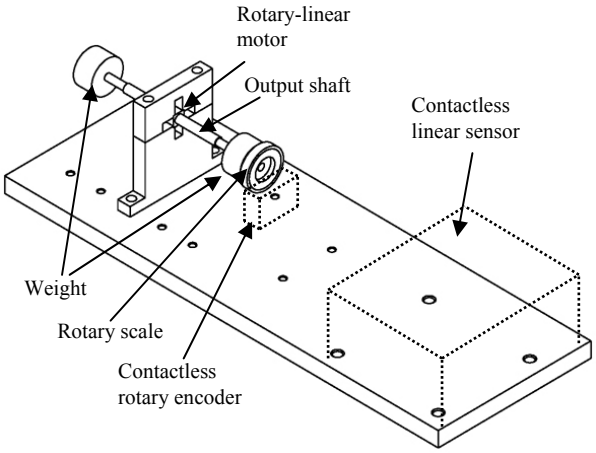

Fig.8 Schematic of experimental setup

the velocities, accelerations, and forces can be calculated.

IV. Experimental Results

A. Impedance of the stator

The impedance characteristics of the stator were measured by an impedance analyzer (Agilent Technologies: 4294A). The corners of the stator were fixed softly on a holder, which connects to ground. One of the cables was chosen arbitrary and was connected to the impedance analyzer. Fig.9 shows the impedance and the frequency characteristics at 230-330 kHz. In Fig.9, two resonances were observed at approximately 280 kHz and about 310 kHz. They are natural frequencies at which the motor generates rotary and linear motions respectively. There are two natural frequencies of T_1 and T_2 modes at 310 kHz redundantly. The difference between the measured resonant frequencies and the results of characteristic analysis using FEM was approximately 10 kHz or approximately 3%. This is due to the condition of the stator, such as material inhomogeneity, and discrepancies in the size.

B. Outputs of the rotary-linear motor

Figs.10 and 11 show rotary and linear performances of the motor, including velocities, accelerations, and forces. In the rotation, the rotational speed is stable at approximately 12 rad/s after duration of 1.5 seconds. Here the inertia is the sum of the shaft, weights, and rotary scale. From eq.(1), the maximum torque was 0.07 μNm. By comparison with the torque in a previous work, a value of 0.07 μNm is acceptable. Reference [8] report the cylindrical stator having similar volume, for which a rotational ultrasonic motor generated 0.025μNm at 40 $V_{p\text{-}p}$. For linear motion, the linear speed was reduced at the center of gravity of the shaft with weights. This is because the amplitude of the center of the stator is lower than that of both edges, in view of the linear principle. When the center of gravity of the shaft is positioned at the center of the stator, the shaft loses the linear speed. In other words, if the center of gravity is away from the center of the stator, the preload between the stator and the shaft at the edges is larger. Better performance at linear motion occurs when the center of gravity is away from the center of the stator. The maximum thrust force was 0.05 mN by calculation using eq.(2). Ref. [7] report a linear piezoelectric actuator generates 30mN as the sliding force at 40 $V_{p\text{-}p}$. In the cases of both references ([8] and [7]), optimal preloads have been given to obtain the maximum torque. The torque and thrust force of the rotary-linear motor will be improved by the preload. There is obvious scope to improve the torque and thrust force by refining the structure of the stator, and the friction between the stator and output shaft. Additionally, it was confirmed that the rotary and linear directions are reversible when the voltages are reversed.

C. Effect from frequencies and applied voltages

The frequency and applied voltages as related to performances are essential factor for control of the rotary and linear motions and for designing improvement to performance. The characteristics of conventional micro ultrasonic motor are set out in previous researches [6]. The performance peaks at the resonant frequency, and is movable near that frequency. Fig.12 graphs frequency versus performance; the movable range of the rotary motion is 262-284 kHz. The peak was obtained at approximately 270 kHz. The maximum rotary speed was 260 rpm. On the other hand, the movable range of the linear motion is 300-312 kHz, the maximum linear speed was 50 mm/s at 306 kHz. Fig.13 graphs applied voltage versus performance. It is known that the performance generally increase in proportion to the applied voltages increase [6]. The rotary-linear motor started to move at a voltage of approximately 30 V_{rms} in the both directions. The both of rotary and linear speed increased in proportion to the voltage as the voltage increased. The maximum performances measured were 600 rpm and 120 mm/s at the voltage of 71 V_{rms}. The torque also should increases as the voltages increase, according to Ref. [8].

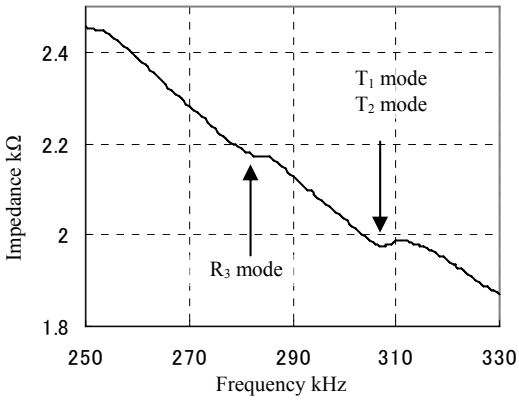

Fig.9 Characteristic frequencies of rotary and linear motion

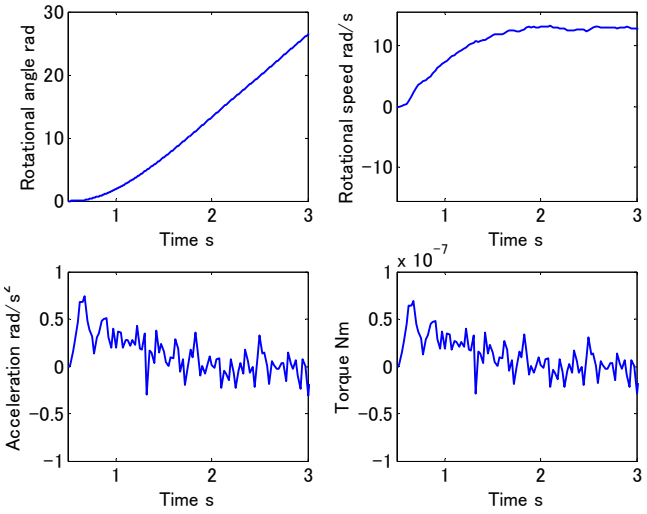

Fig.10 Rotary performances

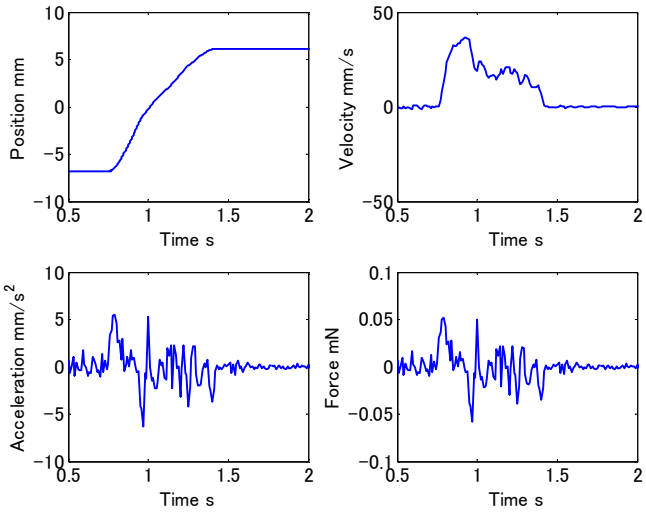

Fig 11 Linear performances

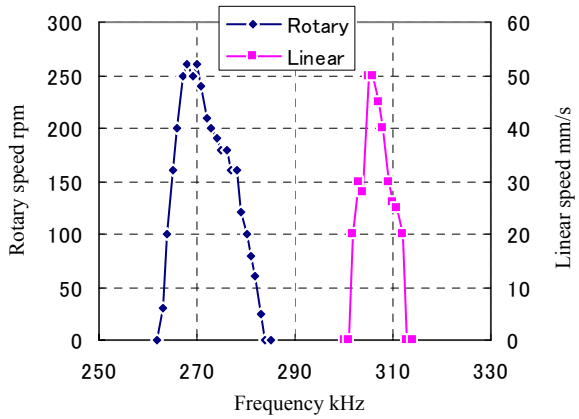

Fig 12 Relationship between the frequency and the performances

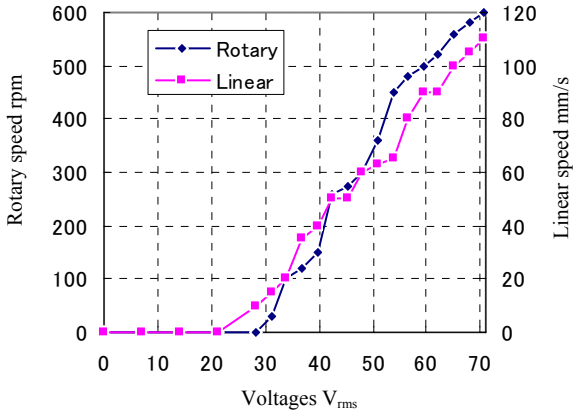

Fig 13 Relationship between the applied voltage and performances

V. Conclusion

We have reported the development of a two-DOF (rotary-linear) actuator using a single metal stator. This rotary-linear motor was miniaturized to a smaller size than hitherto, as a multi-DOF actuator. The stator was fabricated as a 3.5 millimeter cube without a special machining process. The circumference-excited R_3 mode was successfully actuated to rotate the shaft. The T_1 and T_2 modes allowed linear motion of a linear piezoelectric actuator. In rotary motion, a performance of approximately 260 rpm and 0.1 mNm was obtained at the resonant frequency of 270 kHz, and for linear motion the performance was about 50 mm/s and 0.01 mN at 306 kHz when the applied voltages was 42 V_{rms}, though the motor began to rotate at 28 V_{rms}. Since the aim is to operate this rotary-linear motor in a blood vessel, it should be designed so as to rotate at lower voltages of less than 10V.

In the future, further miniaturization and improvement of performance should be possible. In general, ultrasonic motors employ a stator with many slits, and coating of contact surface to obtain higher performance. These should improve the outputs. On the other hand, the combination of the rotary and linear modes can generate other motion, such as helical motion. As well as other medical applications, we foresee microrobotic and industrial applications. Because of the simple parts and structure, the rotary-linear motor is likely to find many applications.

References

[1] S. Guo, T. Fukuda, T. Nakamura, F. Arai, K. Oguro, and M. Negoro, "Micro active guide wire catheter system-Characteristic evaluation, electrical model and operability evaluation of micro active catheter," in *Proc. IEEE International Conference on Robotics and Automation*, 1996, pp. 2226-2231 vol.3.

[2] Y. Haga, Y. Tanahashi, and M. Esashi, "Small diameter active catheter using shape memory alloy," in *Proc. The Eleventh Annual International Workshop on Micro Electro Mechanical Systems* 1998, pp. 419-424.

[3] K. Ikuta, H. Ichikawa, K. Suzuki, and D. Yajima, "Multi-degree of freedom hydraulic pressure driven safety active catheter," in *Proc. IEEE International Conference on Robotics and Automation*, 2006, pp. 4161-4166.

[4] R. D. Safian, M. S. Freed, C. Grines, and M. Freed, *The Manual of Interventional Cardiology*: Physicians Press 2001.

[5] T. Wada, A. Nakajima, T. Moriya, and Y. Furukawa, "Development of IVUS (Intravascular Ultrasound) Driven by Ultrasonic Micromotor —Principle of Drive and Detection Methods—," in *The 11th International Conference on Precision Engineering*, 2006, pp. 113-116.

[6] T. Morita, M. Kuribayashi Kurosawa, and T. Higuchi, "A cylindrical micro ultrasonic motor using PZT thin film deposited by single process hydrothermal method (φ2.4 mm, L=10 mm stator transducer)," *IEEE Trans. Ultrasonics, Ferroelectrics and Frequency Control,* vol. 45, pp. 1178-1187, 1998.

[7] J. Friend, Y. Gouda, K. Nakamura, and S. Ueha, "A simple bidirectional linear microactuator for nanopositioning - the "Baltan" microactuator," *IEEE Trans. Ultrasonics, Ferroelectrics and Frequency Control,* vol. 53, pp. 1160-1168, 2006.

[8] T. Kanda, A. Makino, T. Ono, K. Suzumori, T. Morita, and M. K. Kurosawa, "A micro ultrasonic motor using a micro-machined cylindrical bulk PZT transducer," *Sensors and Actuators A: Physical,* vol. 127, pp. 131-138, 2006.

[9] K. Chinzei, R.Kikinis, and F.Jolesz, "MR Compatibility of Mechatronic Devices: Design Criteria," in *Proc. MICCAI '99 Lecture Notes in Computer Science*, 1999, pp. 1020-1031.

[10] A. B. de Gonzalez and S. Darby, "Risk of cancer from diagnostic X-rays: estimates for the UK and 14 other countries," *The Lancet,* vol. 363, pp. 345-351, 2004.

[11] T. Funakubo, T. Tsubata, Y. Taniguchi, K. Kumei, T. Fujimura, and C. Abe, "Ultrasonic Linear Motor Using Multilayer Piezoelectric Actuators," *Japanese journal of applied physics. Pt. 1, Regular papers & short notes,* vol. 34, pp. 2756-2759, 1995.

[12] T. Hemsel, M. Mracek, J. Twiefel, and P. Vasiljev, "Piezoelectric linear motor concepts based on coupling of longitudinal vibrations," *Ultrasonics,* vol. 44, pp. e591-e596, 2006.

[13] K. Takemura and T. Maeno, "Design and control of an ultrasonic motor capable of generating multi-DOF motion," *IEEE/ASME Transactions on Mechatronics,* vol. 6, pp. 499-506, 2001.

[14] M. Aoyagi, S. P. Beeby, and N. M. White, "A novel multi-degree-of-freedom thick-film ultrasonic motor," *IEEE Trans. Ultrasonics, Ferroelectrics and Frequency Control,* vol. 49, pp. 151-158, Feb. 2002.

[15] K. Nakamura, M. Kurosawa, H. Kurebayashi, and S. Ueha, "An estimation of load characteristics of an ultrasonic motor by measuring transient responses," *IEEE Trans. Ultrasonics, Ferroelectrics and Frequency Control,* vol. 38, pp. 481-485, 1991.